Filter-based reconstruction methods for tomography
Pelt, D.M.

Citation
Pelt, D. M. (2016, May 3). *Filter-based reconstruction methods for tomography*. Retrieved from https://hdl.handle.net/1887/39638

Cover Page

The handle http://hdl.handle.net/1887/39638 holds various files of this Leiden University dissertation.

Author: Pelt D.M.
Title: Filter-based reconstruction methods for tomography
Issue Date: 2016-05-03

6

Application of NN-FBP in Electron Tomography

6.1 Introduction

Gold nanoparticles (NPs) have truly unique electronic, optical as well as catalytic properties, rendering them ideal for numerous applications in fields as diverse as photovoltaics, optoelectronics and biomedicine [ZCG09; ZO11; RM05; CL14]. Furthermore, gold NPs can be prepared with almost any desired shape. Crucial to their application, however, is their exact structure, and specifically their anisotropy as well as the surface facets they expose. Currently, it is empirically understood how particle size and shape may be controlled during synthesis [Pér+05; Grz+08; Sán+06; THY08]. Although transmission electron microscopy (TEM) has become a routine tool to investigate e.g. particle size, (atomic) structure and shape, increasingly advanced TEM is required for a more in-depth characterization. For example, the surface facets of Au nanorods have a major influence on crucial effects such as reactivity and ligand adsorption and there has been controversy regarding facet indexing [Pec+08; Car+10; Kat+10]. Indeed, TEM images are only two-dimensional (2D) projections of three-dimensional (3D) objects. To overcome this problem, 3D electron microscopy, or "electron tomography" was developed [Kos+97; Fra92]. In 2003, Paul Midgley and co-workers demonstrated the potential of the technique in materials science based on high angle annular dark field scanning transmission electron (HAADF-STEM) microscopy [MW03; MD09]. Since

---

This chapter is based on:

E. Bladt, D. M. Pelt, S. Bals, and K. J. Batenburg. "Electron tomography based on highly limited data using a neural network reconstruction technique". *Ultramicroscopy* 158 (2015), pp. 81–88.

then, different electron microscopy modes have been combined successfully with tomography, leading to a broad variety of 3D structural and compositional information at the nanoscale [Wol+10; Wey+06; Bar+08; MB12; Gor+11; Kos+00]. Very often, electron tomography is used to determine the size and shape of the particles and nowadays, 3D reconstructions can even be obtained with a resolution at the atomic level [Gor+12a; Van+11]. Although these investigations provide very precise information on the NP morphology, both the acquisition of tilt series as well as the 3D reconstruction is very time consuming and it is consequently not straightforward to acquire results in 3D that are statistically relevant, which is a major drawback e.g. when using electron tomography to optimize the synthesis of NPs. This problem will be even more essential for anisotropic NPs that are currently receiving a lot of attention because of the increased flexibility they provide to tune the final (optical) properties [GS07; NPK10; GGL12]. Since the optimization of the production of NPs with a specific shape would largely benefit from statistical 3D results with a nanometer resolution, one of the emerging challenges in the field of electron tomography is to increase the throughput of 3D reconstructions of NPs. At the same time, the quality of the reconstructions should be maintained and should enable one to obtain reliable and quantitative results concerning parameters such as particle size and surface morphology.

In this chapter, we will determine the 3D shape and size of a large set of anisotropic Au NPs. We will make effective use of a new approach for electron tomographic reconstructions that is based on artificial neural networks. The neural network filtered backprojection method (NN-FBP) is a recently developed reconstruction technique that has been applied successfully to X-ray tomography (see Chapter 5); however the implementation for electron tomography is completely new. The method that we propose will enable us to reduce the number of necessary projection images for a 3D reconstruction by a factor of 5 or more. In this manner, the acquisition time and time that is necessary for a 3D reconstruction is significantly reduced, enabling 3D results that are of statistical relevance.

6.2 Neural network filtered backprojection method

The sample that was investigated contains Au NPs yielding different morphologies: nanorods, nanotriangles, nanoprisms and nanospheres. An HAADF-STEM overview image of the sample is provided in Fig. 6.1.a. Although this image only corresponds to a 2D projection of a set of 3D objects, it is already clear that different morphologies occur. In conventional electron tomography, a large set of 2D projection images is acquired from the same region of interest over a large tilt range with a tilt increment of typically 1° or 2°. As all the investigated nanoparticles have a thickness below 100 nm, the projection requirement for tomography is satisfied [MW03; Erc+06]. Once this so-called "tilt series" is aligned, the images serve as an input for a mathematical algorithm that enables one to reconstruct the original 3D structure. Very often, the 3D reconstruction is performed using the "Weighted Backprojection" algorithm (also known as Filtered Backprojection) or using the "Simultaneously Iterative Reconstruction Technique" (SIRT). The outcome of this procedure for the different NPs in Fig. 6.1.a is
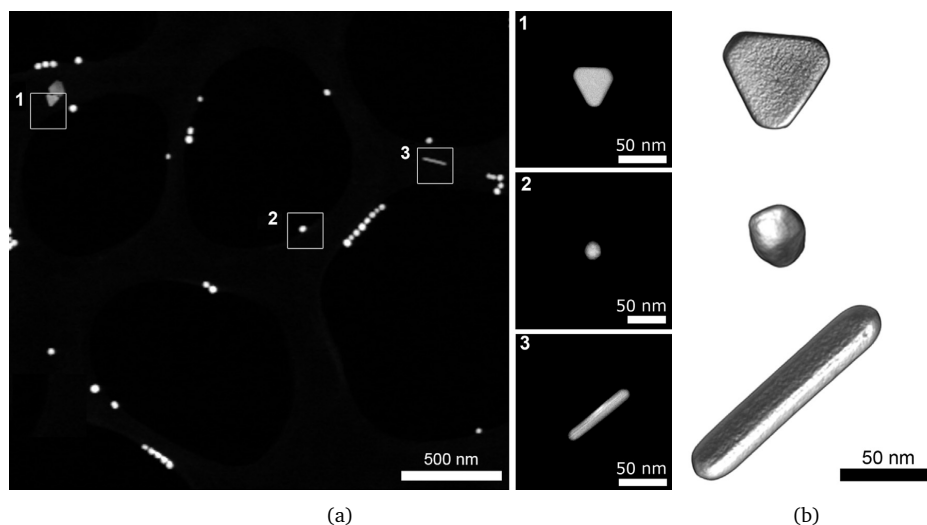
Figure 6.1: (a) The HAADF-STEM overview image shows the presence of several morphologies in the sample, with indication of (1) a nanotriangle, (2) a nanosphere and (3) a nanorod. (b) 3D volume renderings of the corresponding nanoparticles are presented.

visualized in Fig. 6.1.b. The reconstructions are calculated using the SIRT algorithm and are based on a series of 151 images, acquired over a tilt range of $\pm 75°$. Since the quality of 3D reconstructions based on the conventional approach is predominantly determined by the number of projection images [CDK70; Gil72; MVB11], these experiments are very time-consuming and require sufficient measurement time at the TEM.

The key to increasing the image quality if only a small number of 2D projections are available, is the effective use of prior knowledge in the reconstruction. By exploiting rather generic features of the particles, without assuming a specific shape or morphology, this additional knowledge is used to compute a particle shape that better approximates the true morphology. Various algorithms involving prior knowledge are currently in use in electron tomography (e.g. the DART algorithm for discrete tomography [BS11] and multiple methods for Total Variation Minimization [Gor+12b]), where the particular prior knowledge is encoded by the user and various parameters have to be set. These prior-knowledge based methods are typically very time-consuming, which limits the throughput of 3D reconstructions that can be achieved by using them for reconstruction. Furthermore, implementing these methods can be difficult and time-consuming as well, since they rely on advanced mathematics. In this chapter, we propose an alternative approach called Neural Network Filtered Backprojection (NN-FBP), described in Chapter 5 of this thesis, which can effectively exploit sample characteristics to improve reconstruction quality, while still being highly computationally efficient. Here, we apply this new technique for the first time to electron tomography data. The application of NN-FBP to electron tomography consists of two phases: (i) a learning phase, in which full tilt series and their corresponding reconstructions are used to calibrate the

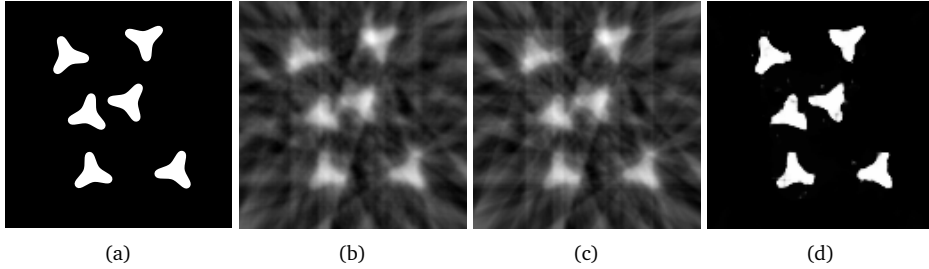|			
(a)	(b)	(c)	(d)

Figure 6.2: Three reconstructions of a phantom image from 10 projections: (a) the phantom image, (b) WBP with a single filter, (c) a linear combination of two WBP reconstructions, and (d) a combination of two WBP reconstructions with a pixel-wise nonlinear scaling operation. In each reconstruction, the weights and filters are chosen such that the mean squared error with the phantom image is minimized.

reconstruction algorithm and (ii) a reconstruction phase, in which large batches of limited tilt series (i.e. using fewer projections) are rapidly reconstructed. In the next subsections, we will first briefly explain how the reconstructions are formed in the reconstruction phase, followed by an overview of how the calibration is performed in the learning phase.

Reconstruction phase

Reconstructions obtained by standard Weighted Backprojection are commonly plagued by a range of reconstruction artifacts when reconstructing from a limited tilt range and few projection angles. Streaks can be observed due to the limited number of projections, and the limited angular range leads to elongation and blurring in the Z-direction. In Chapter 5, it was found that strong improvements on the reconstruction quality from limited data can be obtained by combining a small number (e.g. 2 or 4) of WBP reconstructions, each obtained using a different filter.

In the reconstruction phase, the NN-FBP algorithm computes a reconstructed volume from limited projection data by combining multiple WBP reconstructions with different filters into a single reconstruction. A key ingredient of the algorithm is the application of a pixel-wise nonlinear scaling operation to each of the WBP images. Following this operation, the images are combined by taking a weighted sum of the scaled WBP images. As a final step, another nonlinear scaling operation is applied to this combined image (see reconstruction phase in Fig. 6.3).

Note that without these nonlinear scaling operations, the final reconstruction can also be obtained by first creating a weighted sum of the different filters, and performing a Weighted Backprojection with the resulting filter, as the WBP algorithm is a linear method with respect to the used filter. Because of this, such a method will not be able to produce more accurate reconstructions than standard Weighted Backprojection with an appropriately chosen filter. Also, because of the nonlinear scaling operation, it is not possible to directly compare the filters of the NN-FBP method with standard filters for WBP.

By using the nonlinear scaling operation, the NN-FBP algorithm is able to reduce the

artifacts that are usually present in standard Weighted Backprojection reconstructions when only a small number of projections are available. An example image with standard Weighted Backprojection, a linear combination of two Weighted Backprojections, and a combination of two Weighted Backprojections with nonlinear scaling is shown in Fig. 6.2. As expected, the figure shows that the linear combination is identical to a single Weighted Backprojection reconstruction, while the combination with nonlinear scaling is significantly more accurate.

Learning phase

The question remains how the different filters and weights have to be chosen, such that the method produces accurate reconstructions. In Chapter 5, it is shown that ideas from artificial neural network theory can be used to find good filters and weights. Specifically, filters and weights can be learned by the NN-FBP method in a separate learning phase, in which the method is presented with high-quality reconstructions of a set of training objects. In artificial neural network theory, this technique is called supervised learning. In the learning phase, the filters and weights are iteratively adjusted until the NN-FBP reconstructions match the presented high-quality reconstructions. Afterwards, the trained filters and weights can be used to accurately reconstruct objects that are similar to the ones used for training, using only a limited number of projections. The angle distribution of the limited number of projections has to be specified during the learning phase, and the learned filters and weights will be specific to the chosen distribution. To reduce the influence of the specific angles that are chosen, NN-FBP uses angle-independent filters, i.e. the same filters are used for each projection. An important requirement of the NN-FBP method is that the reconstructed objects should consist only of materials that were also present in the training objects. When this requirement is satisfied, the NN-FBP method is able to produce accurate reconstructions, even for objects with different shapes and/or sizes as the training objects. A schematic overview of both the learning phase and subsequent reconstruction of the NN-FBP method is given in Fig. 6.3.

As opposed to previous advanced reconstruction methods, specific prior knowledge is not explicitly used in the NN-FBP method. Instead, the method learns to exploit certain characteristics of the training objects by adjusting the filters and weights appropriately. Because the exploited characteristics are learned automatically by the method, it has a broader applicability than previous advanced 3D reconstruction methods. Also, since NN-FBP is based on the efficient Weighted Backprojection algorithm, it is computationally efficient as well, enabling high throughput of 3D reconstructions. An additional advantage is that existing implementations of the Weighted Backprojection algorithm can be used to easily implement the NN-FBP method. A final advantage is that it is possible to include the segmentation step in the NN-FBP method by using segmented high-quality reconstructions of the training objects in the learning phase. In this case, the NN-FBP method will reconstruct objects with voxel values that are very close to their segmented value, and the final segmentation can be performed by simple rounding to the nearest segmented value. This removes the need for manual segmentation, which can be problematic for other methods when only a limited set of
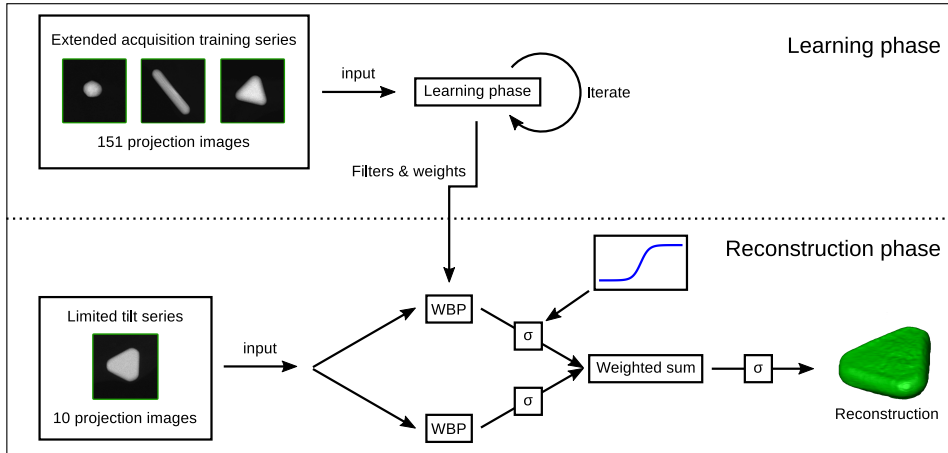
Figure 6.3: Schematic overview of the NN-FBP procedure. In the learning phase, the extended acquisition series are used as an input to learn filters and weights specific to the training objects. In the reconstruction phase, the learned filters are used in multiple WBP reconstructions with an additional pixel-wise nonlinear scaling operation, which are combined to obtain a single reconstruction of a limited tilt series.

projections is available.

6.3 Results

Qualitative results

In a first experiment, tilt series of a nanosphere, a nanorod and a nanotriangle are acquired over an angular tilt range of ± 75° with a tilt increment of 1°. These three series are used as training series, resulting in a set of filters that will be used during the NN-FBP approach. The resulting NN-FBP algorithm is applied to a limited tilt series that was acquired from a different nanotriangle. Although only 10 projection images obtained over a range of ± 75° are used during the NN-FBP reconstruction, it needs to be pointed out that we also acquired an extended series of 151 projection images. The SIRT reconstruction of the extended dataset was used as ground truth, in order to evaluate the NN-FBP outcome. Figure 6.4.a presents a volume rendering of this full range SIRT reconstruction. In all experiments, we used 200 iterations for the SIRT reconstructions, which was empirically verified to produce accurate reconstructions. The result of the NN-FBP algorithm is shown in Fig. 6.4.b. It must be stressed that in this case only 10 projection images were used. It can be seen that the 3D volume visualization of the NN-FBP reconstruction is in very good agreement with the SIRT reconstruction of the full data series. The top and side facet can clearly be distinguished in the corresponding orthoslices in Fig. 6.4.e,i,m and f,j,n. On the other hand, when comparing the SIRT reconstruction based on the extended series with the SIRT reconstruction based on 10 projection images (Fig. 6.4.c,g,k,o), it can
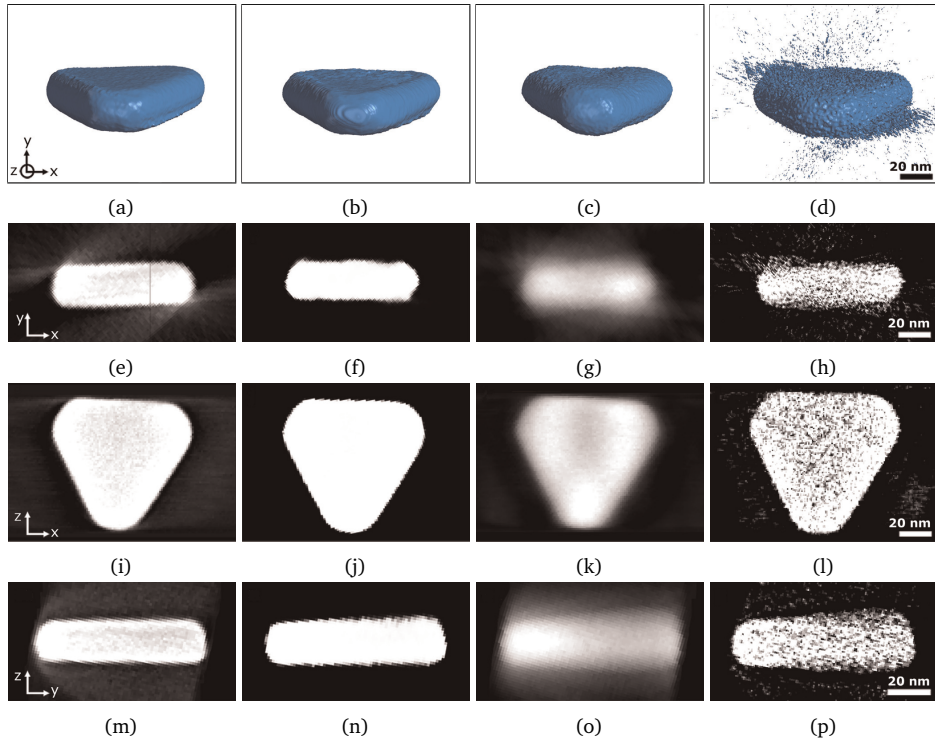
Figure 6.4: Reconstructed volumes of a nanotriangle using (a) the full dataset of 151 projections and the SIRT algorithm, and a limited dataset of only 10 projections using (b) the NN-FBP, (c) the FBP and (d) the SIRT algorithm. Xy, xz and yz orthoslices through the (e,i,m) full SIRT, (f,j,n) the NN-FBP, (g,k,o) the limited SIRT and (h,l,p) the limited WBP reconstructions of the nanotriangle.

be seen that the faceted shape is less pronounced. In the WBP reconstruction applied on 10 projection images (Fig. 6.4.d,h,l,p), severe noise and streaking artifacts can be distinguished. These artifacts can be prohibitive for further analysis of the scanned object, such as volume or shape calculations. Therefore, the WBP reconstruction will be left out in the further analysis. The benefits of NN-FBP become obvious; the number of images required for a 3D reconstruction using NN-FBP is reduced by a factor of 15, but the quality is comparable to a reconstruction based on a full data series with a tilt increment of 1°.

In Fig. 6.5 and Fig. 6.6, results for a nanosphere and a nanorod are presented, respectively. Here, the training of the filters was again obtained by 3 training series. For the nanosphere, extended series of the nanorod and both nanotriangles were used. The training step for the nanorod was performed by the extended series of the nanosphere and both nanotriangles. These nanostructures yield less facets and as a consequence, the general morphology as visualized in Fig. 6.5.b,c and Fig. 6.6.b,c appears to be better preserved when using only 10 projections. However, missing wedge artifacts can be clearly seen in the orthoslices presented in Fig. 6.5.f,i,l and Fig. 6.6.f,i,l. Because
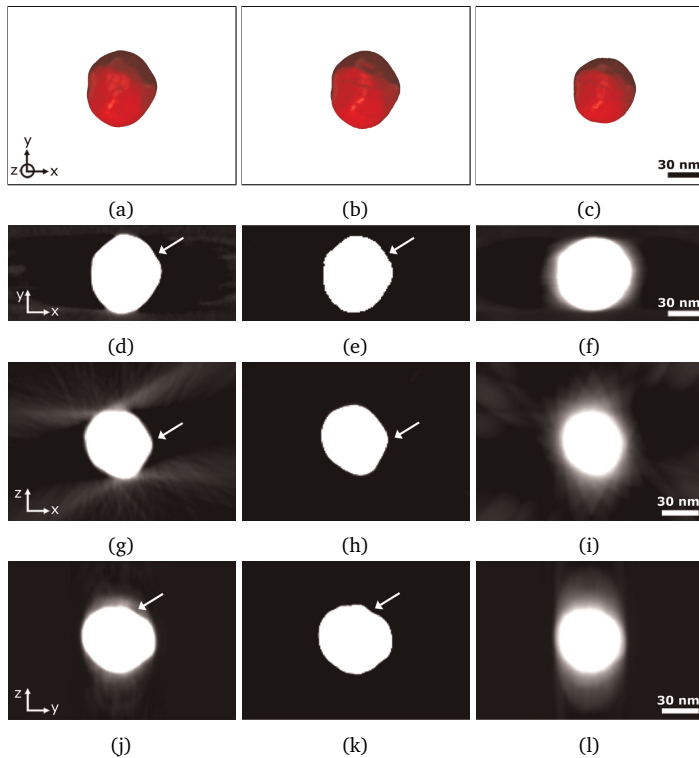
Figure 6.5: Reconstructed volumes of a nanosphere using (a) the full dataset of 151 projections and the SIRT algorithm, and a limited dataset of only 10 projections using (b) the NN-FBP and (c) the SIRT algorithm. Xy, xz and yz orthoslices through the (d,g,j) full SIRT, (e,h,k) the NN-FBP and (f,i,l) the limited SIRT reconstructions of the nanosphere. The white arrows indicate the presence of surface roughnesses. It is clear that these features are visible both in the orthoslices through the full SIRT and in the orthoslices through the NN-FBP reconstruction; however, in the limited SIRT reconstruction they are not detectable.

of such artifacts, some features of the morphology indicated by white arrows in both the orthoslices through the full SIRT reconstruction (Fig. 6.5.d,g,j) and the NN-FBP reconstruction (Fig. 6.5.e,h,k) are not clearly visible in the orthoslices through the limited SIRT reconstruction (Fig. 6.5.f,i,l).

Quantitative results

As a quantitative measure, a difference reconstruction for the nanosphere is constructed by subtracting the SIRT (Fig. 6.7.a) and NN-FBP reconstructions based on 10 projection images (Fig. 6.7.b) from the full SIRT reconstruction of the nanorod. The threshold value for the full SIRT reconstruction is obtained from the histogram. The histogram of the limited SIRT reconstruction, however, is largely influenced by the lack of projection images. In Fig. 6.8, comparisons are shown between the histograms of the full SIRT reconstruction and the limited SIRT reconstruction for each nanoparticle. Clearly, one
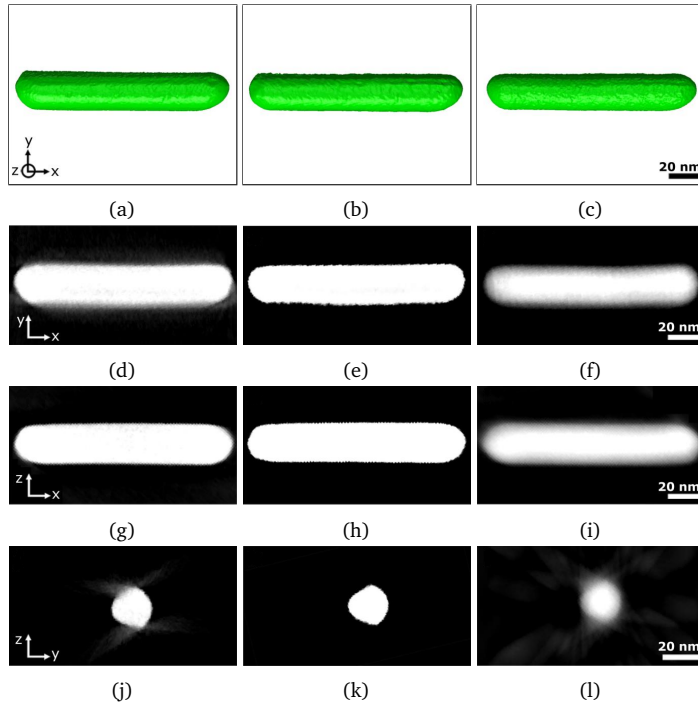
Figure 6.6: Reconstructed volumes of a nanorod using (a) the full dataset of 151 projections and the SIRT algorithm, and a limited dataset of only 10 projections using (b) the NN-FBP and (c) the SIRT algorithm. Xy, xz and yz orthoslices through the (d,g,j) full SIRT, (e,h,k) the NN-FBP and (f,i,l) the limited SIRT reconstructions of the nanorod.
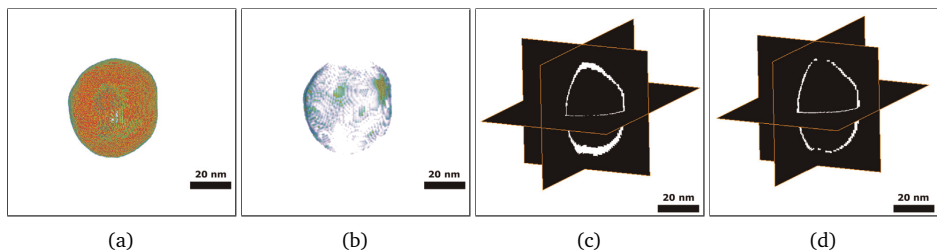

Figure 6.7: Difference reconstructions of the nanosphere constructed by subtracting (a) the SIRT and (b) NN-FBP reconstruction of 10 projection images from the full SIRT reconstruction representing the missing volume and its orthoslices (c) and (d), respectively. The volume misinterpretation for the NN-FBP reconstruction equals only 1.6%, which is indicated by the fine shell of the difference reconstruction. The thicker shell present in the difference reconstruction of the limited SIRT equals a volume misinterpretation of 21.5%.
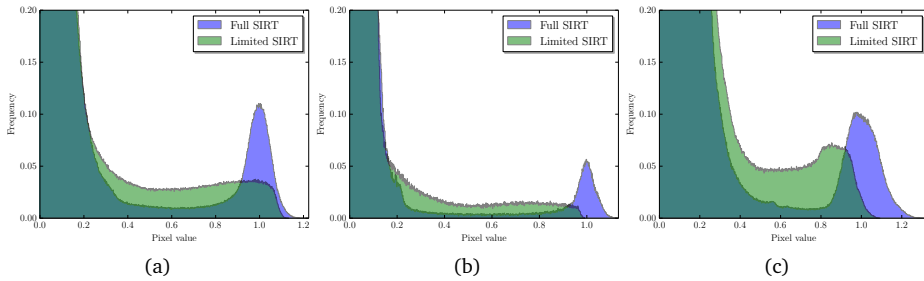
Figure 6.8: Histograms of SIRT reconstructions of the nanorod (a), the nanosphere (b), and the nanotriangle (c), with all 151 projections (Full), and only 10 projections (Limited). It is clear that the poor quality of the limited SIRT reconstruction hampers an objective choice of a threshold for segmentation purposes.
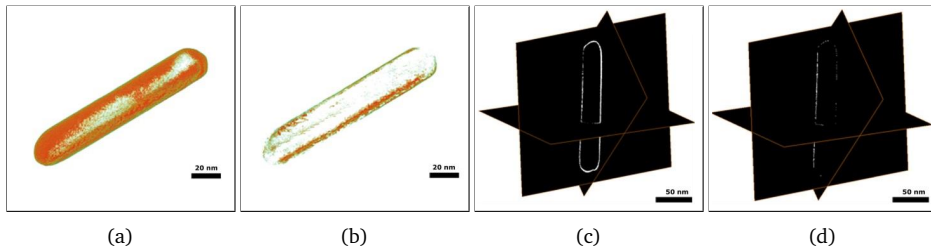

Figure 6.9: Difference reconstructions of the nanorod constructed by subtracting (a) the SIRT and (b) NN-FBP reconstruction of 10 projection images from the full SIRT reconstruction representing the missing volume. Corresponding orthoslices through the difference reconstruction of a nanorod using (c) SIRT and (d) NN-FBP on 10 projections are shown. The volume misinterpretation for the NN-FBP reconstruction equals only 2.3%, which is indicated by the fine shell of the difference reconstruction. The thicker shell present in the difference reconstruction of the limited SIRT equals a volume misinterpretation of 13.1%.
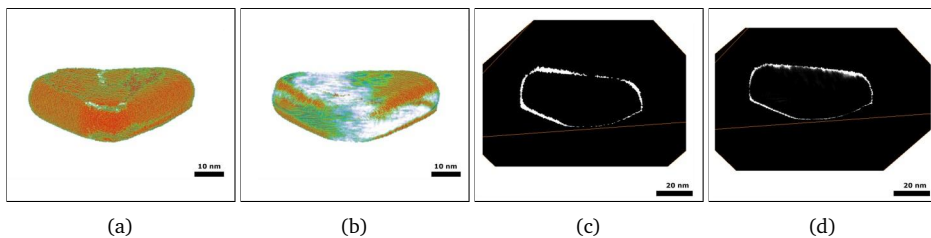

Figure 6.10: Representation of the shape misinterpretation, which for (a) the limited SIRT reconstruction shows a volume underestimation at the center of the nanotriangle and a volume overestimation at the tips of the nanotriangle. In (b) the shape misinterpretation for the limited NN-FBP reconstruction is visualized. (c) and (d) represent the orthoslices through the limited SIRT and NN-FBP reconstruction, respectively. The shape misinterpretation for the NN-FBP reconstruction equals 7.5%, which is indicated by the fine shell of the difference reconstruction. The thicker shell present in the difference reconstruction of the limited SIRT equals a shape misinterpretation of 16.5%.
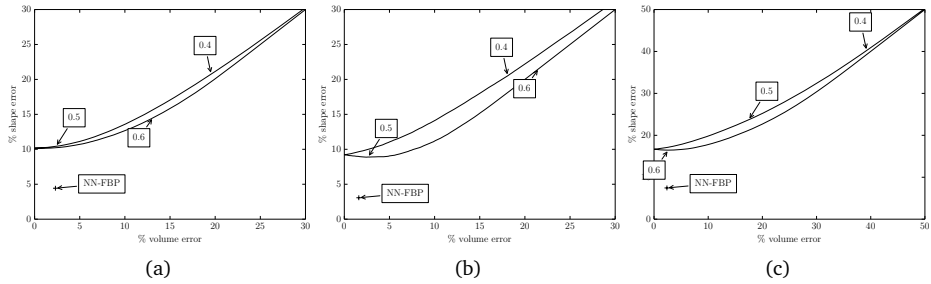
Figure 6.11: Plots of the relative error in the shape and the volume of segmented limited SIRT reconstructions of the nanorod (a), the nanosphere (b), and the nanotriangle (c), compared to the full SIRT reconstruction, for different thresholds of the limited SIRT reconstruction. The error in shape is defined as the number of voxels that are labeled differently in the segmentations of the limited in comparison to the full SIRT reconstruction. The error in volume is defined as the absolute value of the difference between the volumes of the segmented limited SIRT reconstruction and the segmented full SIRT reconstruction. The errors for a threshold of 0.4, 0.5 and 0.6 are indicated with arrows and intermediate thresholds are shown by a line. The errors of the NN-FBP method for each nanoparticle are also shown. Note that for each nanoparticle, the error of the NN-FBP reconstruction is closer to the origin than the error of any thresholded SIRT reconstruction.

would have trouble choosing correct threshold values on the basis of the limited SIRT histograms. Therefore, the same threshold value as the full SIRT reconstruction is used for the limited SIRT reconstructions. Since the NN-FBP reconstructions are already segmented, no threshold value is needed for them. Both from the visualization in Fig. 6.7.a, as well as the corresponding orthoslices through the difference reconstruction in Fig. 6.7.c, the volume misinterpretation of the limited SIRT reconstruction is clearly detectable. The orthoslices through the limited SIRT difference reconstruction of the nanosphere show a thick white shell. Here, the larger amount of white pixels indicates a volume misinterpretation of 21.5% when using the SIRT algorithm on the dataset of only 10 projection images. From Fig. 6.7.b and its corresponding orthoslices in Fig. 6.7.d, it is clear that the volume reconstructed with NN-FBP on 10 projection images is close to the actual volume. The NN-FBP reconstruction has only 1.6% of volume underestimation. For the nanorod (Fig. 6.9), the volume for SIRT applied to a limited dataset results in an underestimation of 13.1%. The NN-FBP reconstruction leads to a misinterpretation of only 2.3%. For the nanotriangle, the volume misinterpretation for the limited SIRT reconstruction equals 2.7%. When reconstructing the 10 projection dataset with the NN-FBP algorithm, the volume misinterpretation equals 2.4%. For the nanotriangle, the volume misinterpretation of the limited SIRT reconstructions is close to the misinterpretation of the NN-FBP reconstruction. In this case, however, the volume misinterpretation of the limited SIRT reconstruction gives a misleading result, due to a volume underestimation at the center of the nanotriangle and a volume overestimation at the tips of the nanotriangle. In general, the volume misinterpretation can be misleading due to the canceling out of overestimation and underestimation. Clearly, the evaluation of the quality of the reconstruction can not only be based on an inspection of the volume error. Therefore, the shape error is introduced, which corresponds to the number of voxels that are labeled differently in the segmentations
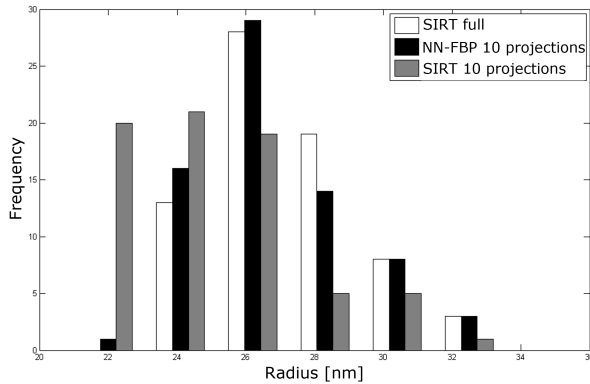
Figure 6.12: Distribution of the radii of nanospheres reconstructed using SIRT on full datasets of 151 projections (white), NN-FBP (black) and SIRT on limited datasets of 10 projections (gray). The distributions of SIRT full and NN-FBP 10 projections are in good agreement. When SIRT is applied on the limited datasets, a different distribution is found due to the misinterpretation of the volume.

of the limited data reconstructions in comparison to the full SIRT reconstruction. In this manner, both the local volume underestimation at the center as well as the volume overestimation at the tips is taken into account. For the nanotriangle, there is a 16.5% shape misinterpretation for the limited SIRT reconstruction (Fig. 6.10). The shape error for the NN-FBP reconstruction equals 7.5%, which is clearly smaller in comparison to the shape error of the limited SIRT reconstruction. An extended investigation of the influence of the chosen threshold value on the shape error and volume error of the limited SIRT reconstructions is shown in Fig. 6.11. Note that from Fig. 6.11, one can conclude that the errors depend heavily on the chosen threshold value, showing the difficulties one would have when choosing a threshold value both optimizing shape and volume error for limited SIRT reconstructions.

Statistical results

In general it is difficult to obtain statistical results when applying electron tomography. As pointed out previously, the acquisition of tilt series for electron tomography is very time consuming and a large electron dose is required in the case of small tilt increments. The NN-FBP algorithm is therefore of great interest as it can be applied to reduce the acquisition time. In this manner a large set of nanostructures can be investigated in an efficient manner, leading to statistical results. Using the NN-FBP approach explained above, training was performed on a set of 20 nanoparticles, and a total of 71 nanospheres was investigated. The number of nanoparticles to train on was chosen empirically, such that there were both enough particles to use in the learning phase, and enough particles to obtain statistical results from. In Fig. 6.12, the distribution of the radii of these nanospheres is evaluated. In order to investigate the reliability of the NN-FBP approach, extended tilt series of 151 images were acquired for

all particles. The outcome of the NN-FBP algorithm and the SIRT algorithm, using only 10 projections, is then compared to the measurements based on the SIRT reconstruction using 151 projections. The distribution indicated in gray in Fig. 6.12 presents the radii distribution for the nanospheres reconstructed using SIRT applied to limited datasets and clearly gives a different distribution in comparison to the radii distribution of the full SIRT reconstruction, which is presented in white. The average radius found in this manner equals (24.1 ± 0.59) nm, which is significantly smaller than the actual radius which equals (27.1 ± 0.25) nm, found through the full SIRT reconstructions. As the optical properties, such as the absorption cross section, are dependent on the shape and size of the nanoparticles, it is of key importance to retrieve the real nanoparticle morphology. A small difference of a few nanometer can already influence the outcome of the optical response [LE00; Per+10]. The radii distribution of the NN-FBP reconstruction (black), however, is in good agreement with the results extracted from the full SIRT data (white). The average radius of the NN-FBP reconstructed nanospheres equals (26.8 ± 0.29) nm. This value is in good agreement with the actual average radius and shows a clear overlap of the error bars. It is again clear that the SIRT algorithm can not provide reliable information when limited datasets are investigated. These results confirm the reliability of the NN-FBP algorithm and demonstrate the possibility of combining electron tomography and statistical measurements.

6.4 Conclusion

We have shown that the NN-FBP reconstruction algorithm is able to yield electron tomography reconstructions based on highly limited data with a comparable quality to a reconstruction based on a full data series with a tilt increment of 1°. The decrease in acquisition time and the use of an efficient reconstruction method enables us to examine a broad range of nanostructures in a statistical manner. The NN-FBP algorithm also has promising prospects for the 3D investigation of beam sensitive samples, where only a limited amount of projection images need to be acquired.